J|A|C|S
ARTICLES

Published on Web 10/13/2010

A Chelator-Free Multifunctional [^{64}Cu]CuS Nanoparticle Platform for Simultaneous Micro-PET/CT Imaging and Photothermal Ablation Therapy

Min Zhou,[†] Rui Zhang,[†] Miao Huang,[†] Wei Lu,[†] Shaoli Song,[†,§] Marites P. Melancon,[†] Mei Tian,[†] Dong Liang,[‡] and Chun Li*[,†]

Department of Experimental Diagnostic Imaging, The University of Texas MD Anderson Cancer Center, Houston, Texas 77030, United States, and Department of Pharmaceutical Sciences, Texas Southern University, Houston, Texas 77004, United States

Received July 31, 2010; E-mail: cli@mdanderson.org

Abstract: We synthesized and evaluated a novel class of chelator-free [^{64}Cu]CuS nanoparticles (NPs) suitable both for PET imaging and as photothermal coupling agents for photothermal ablation. These [^{64}Cu]CuS NPs are simple to make, possess excellent stability, and allow robust noninvasive micro-PET imaging. Furthermore, the CuS NPs display strong absorption in the near-infrared (NIR) region (peak at 930 nm); passive targeting prefers the tumor site, and mediated ablation of U87 tumor cells occurs upon exposure to NIR light both in vitro and in vivo after either intratumoral or intravenous injection. The combination of small diameter (~11 nm), strong NIR absorption, and integration of ^{64}Cu as a structural component makes these [^{64}Cu]CuS NPs ideally suited for multifunctional molecular imaging and therapy.

Introduction

Positron emission tomography (PET) is a powerful and widely used diagnostic tool that has the advantages of high sensitivity (down to the picomolar level) and the ability to provide quantitative imaging analyses of in vivo abnormalities.[1−3] ^{64}Cu [$t_{1/2}$ = 12.7 h; β^+, 0.653 MeV (17.8%); β^-, 0.579 MeV (38.4%)] has decay characteristics that allow for both PET imaging and targeted radiotherapy for cancer.[4] This nuclide has been investigated as a promising radiotracer for real-time PET monitoring of regional drug concentration, pharmacokinetics, and dosimetry during radiotherapy.[4,5]

Radioisotopes have been introduced into various nanoparticles (NPs), including quantum dots,[6,7] gold NPs,[5,8,9] carbon nanomaterials,[10,11] and polymeric NPs,[12−15] through radionuclide labeling to allow noninvasive in vivo nuclear imaging of the NPs' pharmacokinetics, tissue distribution, and clearance. In several studies, PET has been used to investigate the pharmacokinetics and biodistribution of ^{64}Cu-labeled NPs.[5,13] In all of these studies, the radioisotopes were linked to the NPs through chelators such as diethylenetriaminepentaacetic acid or 1,4,7,10-tetraazacyclododecane-1,4,7,10-tetraacetic acid to form stable complexes.

However, there are two inherent limitations associated with the use of radiometal−chelator complexes for nuclear imaging and in vivo study of NPs.[16] First, the physicochemical properties of NPs attached to radiometal−chelator complexes are not exactly the same as those of NPs without radiotracers. It is well-known that the biodistribution and pharmacokinetic properties of NPs are influenced by their surface properties.[17] Therefore, the data obtained using NPs conjugated with radiometal−chelator complexes may not reflect the pharmacological properties of

[†] The University of Texas MD Anderson Cancer Center.
[‡] Texas Southern University.
[§] On leave from the Department of Nuclear Medicine, Renji Hospital, Shanghai Jiaotong University School of Medicine, Shanghai 200127, P. R. China.

(1) Scheinin, H.; Scheinin, M.; Knuuti, J. *Ann. Med.* **1999**, *31*, 430–431.
(2) Eckelman, W. C. *Drug Discovery Today* **2003**, *8*, 404–410.
(3) Welch, M. J.; Hawker, C. J.; Wooley, K. L. *J. Nucl. Med.* **2009**, *50*, 1743–1746.
(4) Shokeen, M.; Anderson, C. J. *Acc. Chem. Res.* **2009**, *42*, 832–841.
(5) Lu, W.; Zhang, G.; Zhang, R.; Flores, L. G., 2nd; Huang, Q.; Gelovani, J. G.; Li, C. *Cancer Res.* **2010**, *70*, 3177–3188.
(6) Schipper, M. L.; Cheng, Z.; Lee, S. W.; Bentolila, L. A.; Iyer, G.; Rao, J. H.; Chen, X. Y.; Wul, A. M.; Weiss, S.; Gambhirl, S. S. *J. Nucl. Med.* **2007**, *48*, 1511–1518.
(7) Cai, W.; Chen, K.; Li, Z. B.; Gambhir, S. S.; Chen, X. *J. Nucl. Med.* **2007**, *48*, 1862–1870.
(8) Melancon, M. P.; Lu, W.; Yang, Z.; Zhang, R.; Cheng, Z.; Elliot, A. M.; Stafford, J.; Olson, T.; Zhang, J. Z.; Li, C. *Mol. Cancer Ther.* **2008**, *7*, 1730–1739.
(9) Zhang, G.; Yang, Z.; Lu, W.; Zhang, R.; Huang, Q.; Tian, M.; Li, L.; Liang, D.; Li, C. *Biomaterials* **2009**, *30*, 1928–1936.
(10) McDevitt, M. R.; Chattopadhyay, D.; Jaggi, J. S.; Finn, R. D.; Zanzonico, P. B.; Villa, C.; Rey, D.; Mendenhall, J.; Batt, C. A.; Njardarson, J. T.; Scheinberg, D. A. *PLoS One* **2007**, *2*, 1–10.
(11) Liu, Z.; Cai, W. B.; He, L. N.; Nakayama, N.; Chen, K.; Sun, X. M.; Chen, X. Y.; Dai, H. J. *Nat. Nanotechnol.* **2007**, *2*, 47–52.
(12) Pressly, E. D.; Rossin, R.; Hagooly, A.; Fukukawa, K. I.; Messmore, B. W.; Welch, M. J.; Wooley, K. L.; Lamm, M. S.; Hule, R. A.; Pochan, D. J.; Hawker, C. J. *Biomacromolecules* **2007**, *8*, 3126–3134.
(13) Schluep, T.; Hwang, J.; Hildebrandt, I. J.; Czernin, J.; Choi, C. H. J.; Alabi, C. A.; Mack, B. C.; Davis, M. E. *Proc. Natl. Acad. Sci. U.S.A.* **2009**, *106*, 11394–11399.
(14) Yang, Z.; Zheng, S.; Harrison, W. J.; Harder, J.; Wen, X.; Gelovani, J. G.; Qiao, A.; Li, C. *Biomacromolecules* **2007**, *8*, 3422–3428.
(15) Yang, Z.; Leon, J.; Martin, M.; Harder, J. W.; Zhang, R.; Liang, D.; Lu, W.; Tian, M.; Gelovani, J. G.; Qiao, A.; Li, C. *Nanotechnology* **2009**, *20*, 165101.
(16) Sanhai, W. R.; Sakamoto, J. H.; Canady, R.; Ferrari, M. *Nat. Nanotechnol.* **2008**, *3*, 242–244.
(17) Schipper, M. L.; et al. *Small* **2009**, *5*, 126–134.

the unlabeled NPs. Second, the radiometal−chelator complexes may be detached from the surface of the NPs, or the radiometal ions may be displaced in vivo from the radiometal−chelator complexes as a result of transchelation in the presence of high plasma protein concentrations, which again could lead to failure of the in vivo data to reflect the pharmacokinetics and biodistribution of the NPs accurately.[18] Therefore, it is necessary to validate the in vivo data acquired with chelator-based radiolabeling techniques using independent analytical tools.

Photothermal ablation (PTA) therapy has gained increasing attention in recent years as a minimally invasive alternative to conventional approaches for cancer treatment such as surgery and chemotherapy.[19−22] NPs with unique optical properties, primarily gold nanostructures such as gold nanoshells,[23,24] nanorods,[25,26] nanocages,[27,28] and hollow nanospheres[5,8,29] but also carbon nanotubes,[30,31] have been investigated as photothermal coupling agents to enhance the efficacy of PTA therapy. These plasmonic nanomaterials exhibit strong absorption in the near-infrared (NIR) region (λ = 700−1100 nm) and offer the opportunity to convert optical energy into thermal energy, enabling the deposition of otherwise benign optical energy into tumors for thermal ablation of tumor cells.

As a well-known p-type semiconductor material, CuS is of great interest for use in catalysis and photovoltaics. Several methods have been developed for the preparation of copper sulfide NPs.[32−34] Semiconductor CuS NPs are a new class of promising photothermal coupling agents. In our previous work, we synthesized thioglycolic acid-stabilized CuS NPs and demonstrated their application for photothermal destruction of tumor cells in vitro using an NIR laser beam centered at 808 nm.[35] In the current study, we developed a process for the rapid synthesis of radioactive [^{64}Cu]CuS NPs in which ^{64}Cu is an integral building block of CuS rather than chelated to the NPs. Both citrate (Cit)- and polyethylene glycol (PEG)-stabilized [^{64}Cu]CuS NPs were evaluated for their pharmacokinetics and biodistribution. We demonstrated in vivo passive targeting of the nanoparticles to tumors. We further investigated the photothermal killing effect of PEG-stabilized CuS NPs both in vitro and in vivo following intratumoral (i.t.) or intravenous (i.v.) injection. To the best of our knowledge, this is the first report on the use of chelator-free NPs for PET imaging and the first demonstration of the use of CuS NPs for dual imaging and PTA therapy in vivo.

Experimental Section

Materials. Copper(II) chloride ($CuCl_2$), sodium sulfide ($Na_2S\cdot 9H_2O$), sodium citrate, and methoxy-PEG-thiol (SH-PEG; molecular weight 5000 Da) were purchased from Sigma-Aldrich (St. Louis, MO). Isoflurane was obtained from Baxter (Deerfield, IL). $^{64}CuCl_2$ was obtained from the University of Wisconsin (Madison, WI). PD-10 columns were purchased from Amersham-Pharmacia Biotech (Piscataway, NJ). All of the chemicals and solvents were at least ACS-grade and used without further purification. Deionized water (18 MΩ) was obtained from a Milli-Q synthesis system (Millipore, Billerica, MA). Human U87 glioblastoma cells were obtained from American Type Culture Collection (Manassas, VA). RPMI-1640 culture medium and calcein AM were obtained from Sigma-Aldrich.

Synthesis of CuS NPs. The general procedure for the synthesis of CuS NPs in water was as follows. Into 1000 mL of an aqueous solution containing $CuCl_2$ (0.1345 g, 1 mmol) and sodium citrate (0.2 g, 0.68 mmol) was added 1 mL of sodium sulfide solution (Na_2S, 1 M) with stirring at room temperature. The pale-blue $CuCl_2$ solution turned dark-brown immediately upon the addition of sodium sulfide. After 5 min, the reaction mixture was heated to 90 °C and stirred for 15 min until a dark-green solution was obtained. The mixture was transferred to ice-cold water. The citrate-coated CuS NPs (Cit−CuS NPs) were obtained and stored at 4 °C. To introduce the PEG coating, ∼1 mg of SH-PEG was added to the Cit−CuS NP solution (1.42×10^{15} NPs in 1.0 mL of water). The reaction was allowed to proceed overnight at room temperature, affording PEG-coated CuS NPs (PEG−CuS NPs).

Characterizations of CuS NPs. For transmission electron microscopy (TEM), an aqueous solution of CuS NPs was deposited on carbon-enhanced copper grids without negative staining. The NPs were allowed to adhere to the grid for 1 h, after which they were briefly rinsed with deionized water and air-dried. The samples were then examined using a transmission electron microscope (JEM 2010, JEOL, Japan) at an accelerating voltage of 200 kV. Digital images were obtained using an AMT imaging system (Advanced Microscopy Techniques Corp., Danvers, MA). The average diameter of the CuS NPs was determined by measurements on up to 200 individual NPs. UV−vis spectra of CuS NPs were recorded on a Beckman Coulter DU-800 UV−vis spectrometer (Brea, CA) with a 1.0 cm optical path length quartz cuvette. The identity and crystallinity, crystalline structure, size, and shape of the NPs were observed by X-ray diffraction (XRD) and a high-resolution (HR) transmission electron microscope (200 kV, JEOL, Japan). XRD was performed using a Siemens Kristalloflex 810 D-500 X-ray diffractometer (Siemens, Germany) in an operating mode of 40 kV and 30 mA with λ = 1.5406 Å radiation.

Stability of CuS NPs. The stabilities of Cit−CuS and PEG−CuS NPs in various media were investigated by incubating CuS NPs in water, 0.4 mM citrate solution, 100 mM acetate buffer solution, 100 mM NaCl solution, 4-(2-hydroxyethyl)-1-piperazineethane-

(18) Bass, L. A.; Wang, M.; Welch, M. J.; Anderson, C. J. *Bioconjugate Chem.* **2000**, *11*, 527–532.
(19) Amin, Z.; Donald, J. J.; Masters, A.; Kant, R.; Steger, A. C.; Bown, S. G.; Lees, W. R. *Radiology* **1993**, *187*, 339–347.
(20) Nolsoe, C. P.; Torppedersen, S.; Burcharth, F.; Horn, T.; Pedersen, S.; Christensen, N. E. H.; Olldag, E. S.; Andersen, P. H.; Karstrup, S.; Lorentzen, T.; Holm, H. H. *Radiology* **1993**, *187*, 333–337.
(21) Fiedler, V. U.; Schwarzmaier, H. J.; Eickmeyer, F.; Muller, F. P.; Schoepp, C.; Verreet, P. R. *J. Magn. Reson. Imaging* **2001**, *13*, 729–737.
(22) Vogel, A.; Venugopalan, V. *Chem. Rev.* **2003**, *103*, 577–644.
(23) Hirsch, L. R.; Stafford, R. J.; Bankson, J. A.; Sershen, S. R.; Rivera, B.; Price, R. E.; Hazle, J. D.; Halas, N. J.; West, J. L. *Proc. Natl. Acad. Sci. U.S.A.* **2003**, *100*, 13549–13554.
(24) Loo, C.; Lowery, A.; Halas, N.; West, J.; Drezek, R. *Nano Lett.* **2005**, *5*, 709–711.
(25) Dickerson, E. B.; Dreaden, E. C.; Huang, X. H.; El-Sayed, I. H.; Chu, H. H.; Pushpanketh, S.; McDonald, J. F.; El-Sayed, M. A. *Cancer Lett.* **2008**, *269*, 57–66.
(26) Park, J. H.; von Maltzahn, G.; Xu, M. J.; Fogal, V.; Kotamraju, V. R.; Ruoslahti, E.; Bhatia, S. N.; Sailor, M. J. *Proc. Natl. Acad. Sci. U.S.A.* **2010**, *107*, 981–986.
(27) Chen, J. Y.; Wang, D. L.; Xi, J. F.; Au, L.; Siekkinen, A.; Warsen, A.; Li, Z. Y.; Zhang, H.; Xia, Y. N.; Li, X. D. *Nano Lett.* **2007**, *7*, 1318–1322.
(28) Au, L.; Zheng, D. S.; Zhou, F.; Li, Z. Y.; Li, X. D.; Xia, Y. N. *ACS Nano* **2008**, *2*, 1645–1652.
(29) Lu, W.; Xiong, C.; Zhang, G.; Huang, Q.; Zhang, R.; Zhang, J. Z.; Li, C. *Clin. Cancer Res.* **2009**, *15*, 876–886.
(30) Chakravarty, P.; Marches, R.; Zimmerman, N. S.; Swafford, A. D. E.; Bajaj, P.; Musselman, I. H.; Pantano, P.; Draper, R. K.; Vitetta, E. S. *Proc. Natl. Acad. Sci. U.S.A.* **2008**, *105*, 8697–8702.
(31) Burke, A.; et al. *Proc. Natl. Acad. Sci. U.S.A.* **2009**, *106*, 12897–12902.
(32) Haram, S. K.; Mahadeshwar, A. R.; Dixit, S. G. *J. Phys. Chem.* **1996**, *100*, 5868–5873.
(33) Xu, L. M.; Chen, X.; Ma, L.; Gao, F. Q. *Colloids Surf., A* **2009**, *349*, 69–73.
(34) Huang, P.; Li, Z. M.; Hu, H. Y.; Cui, D. X. *J. Nanomater.* **2010**, 1–6.
(35) Li, Y. B.; Lu, W.; Huang, Q.; Huang, M.; Li, C.; Chen, W. *Nanomedicine*, in press.

sulfonic acid (HEPES) buffer, phosphate-buffered saline (PBS), 50 mM bovine serum albumin solution, PBS containing 10% fetal bovine serum (FBS), or 100% FBS at 37 °C for up to 7 days. The appearance of precipitation was observed by visual inspection.

Synthesis of Radioactive [^{64}Cu]CuS NPs. $^{64}CuCl_2$ (20 μL, 1000 μCi) was added to 1 mL of $CuCl_2$ solution (1 mM) containing sodium citrate (0.2 g/L), after which 10 μL of sodium sulfide solution (100 mM) was added to the $CuCl_2$ solution with stirring. The mixture was then heated to 90 °C for 15 min until a dark-green solution was obtained. The reaction mixture was transferred to ice-cold water to give Cit−[^{64}Cu]CuS NPs. The same procedure as for Cit−[^{64}Cu]CuS NPs was used for the preparation of PEG−[^{64}Cu]CuS NPs. Thus, 10 μL of sodium sulfide solution was added to 1 mL of an aqueous solution of $^{64}CuCl_2/CuCl_2$ containing 1 mg of SH-PEG.

The radiolabeling efficiency and stability of labeled NPs were analyzed using instant thin-layer chromatography (ITLC). The ITLC strips were developed with PBS (pH 7.4) containing 4 mM ethylenediaminetetraacetic acid and quantified using an IAR-2000 TLC imaging scanner (Bioscan, Washington, DC). To study the labeling stability, Cit−[^{64}Cu]CuS NPs and PEG−[^{64}Cu]CuS NPs were suspended in PBS or mouse serum and incubated at 37 °C for 24 h. Free $^{64}Cu^{2+}$ ions moved to the solvent front, and the NPs remained at the original spot. The radioactivity at the original spot was recorded as a percentage of the total radioactivity of the ITLC strip.

Pharmacokinetics. All experiments involving animals were done in accordance with the guidelines of the Institutional Animal Care and Use Committee. For pharmacokinetic analysis, mice were intravenously injected with radioactive CuS NPs (4×10^{11} particles, 50 μCi/mouse in 0.2 mL), and blood samples (10 μL) were collected from the tail vein at predetermined time points. The blood pharmacokinetic parameters of the radiotracer were analyzed with a two-compartmental model using WinNonlin 5.0.1 software (Pharsight Corporation, Palo Alto, CA). The animals were euthanized by CO_2 exposure at the end of the study.

Biodistribution Radioactivity Counting. Human U87 glioblastoma tumors were grown subcutaneously in the right thigh of nude mice (20−25 g; Harlan Sprague Dawley, Indianapolis, IN) by injecting 1×10^6 viable tumor cells suspended in PBS. When tumors had grown to 5−8 mm in diameter, the mice were randomly allocated into two groups ($n = 5$). Mice in group 1 were injected with Cit−[^{64}Cu]CuS NPs, and mice in group 2 were injected with PEG−[^{64}Cu]CuS NPs, each at a dose of 8×10^{10} particles per mouse (20 μCi per mouse in 0.2 mL). Mice were killed by CO_2 overexposure 24 h after injection. Blood, heart, liver, spleen, kidney, lung, stomach, intestine, muscle, bone, brain, and tumor tissues were removed and weighed, and radioactivity was measured with a Packard Cobra γ counter (Ramsey, MN). Uptakes of ^{64}Cu-labeled CuS NPs in various organs were expressed as percentages of injected dose per gram of tissue (%ID/g).

Micro-PET/CT Imaging. Mice bearing U87 tumors were prepared as described above. When the tumors reached 8−10 mm in diameter, mice ($n = 3$) were treated with an i.v. injection of PEG−[^{64}Cu]CuS NPs (8×10^{10} particles/mouse, 200 μCi/mouse; 0.2 mL). The animals were anesthetized with 2% isoflurane and placed in the prone position, and micro-PET/CT images were acquired at 1, 6, and 24 h after injection of the radiolabeled nanoparticles using an Inveon micro-PET/CT scanner (Siemens Preclinical Solution, Knoxville, TN). The micro-PET and CT images were generated separately and then fused using Inveon Research Workplace (Siemens Preclinical Solution, Knoxville, TN). For data analysis, the region of interest (ROI) was manually drawn covering the whole tumor on the CT images and copied to the corresponding PET images. Similarly, a circular region of interest was drawn on the muscle of the opposite leg of the mouse on the CT images and copied to the PET images. The mean signal intensities of the tumor and muscle in the ROIs were recorded. The tumor-to-muscle ratio was calculated by dividing the signal intensity of the tumor by that of the muscle.

Photothermal Effect in Aqueous Solution. The laser was a continuous-wave GCSLX-05-1600 m-1 fiber-coupled diode laser with a center wavelength of 808 ± 10 nm. It was powered by a DH 1715A-5 dual-regulated power supply (15PLUS Laser, Diomed, Andover, MA). A 5 m, 600 μm core BioTex LCM-001 optical fiber (BioTex Inc., Houston, TX) was used to transfer laser power from the laser unit to the target. This fiber had a lens mounted at the output that allowed the laser spot size to be changed by changing the distance from the output to the target. The output power was independently calibrated using a hand-held model 840-C optical power meter (Newport Corporation, Irvine, CA) and found to be 1 W for a spot diameter of 3.5 mm (~8 W/cm^2) and a 2 A supply current. The end of the optical fiber was attached to a retort stand using a movable clamp and positioned directly above the sample cell. For measurement of temperature change mediated by CuS NPs, NIR laser light (808 nm) was delivered through a quartz cuvette containing the CuS NPs (100 μL). A thermocouple was inserted into the solution perpendicular to the path of the laser light. The temperature was measured over 10 min. Water was used as a control.

Photothermal Ablation of Cancer Cells with CuS NPs in Vitro. U87 cells were seeded onto a 96-well plate with a density of 10 000 per well 1 day before the experiment. Cells were washed three times with Hanks balanced salt solution (HBSS, Sigma-Aldrich) and then incubated with PEG−CuS NPs in RPMI-1640 culture medium (Invitrogen, Carlsbad, CA) at a CuS concentration of 100 or 500 μM at 37 °C. Cells without NPs were used as a control. After 2 h, the culture medium was replaced with fresh RPMI-1640 medium without phenol red, and the cells were irradiated with a diode NIR laser centered at 808 nm at an output power of 0, 16 W/cm^2 for 5 min, 40 W/cm^2 for 5 min, or 40 W/cm^2 for 2 min. The laser was coupled to a 1 m, 2 mm core fiber that delivered a circular laser beam 4 mm in diameter covering the central area of the microplate well. Power calibration was done automatically. After treatment, cells were resupplied with RPMI-1640 containing 10% FBS. After 24 h, the cells were washed with HBSS and stained with calcein AM for visualization of viable cells according to manufacturer's suggested protocol (Invitrogen). Cells were examined under a Zeiss Axio Observer.Z1 fluorescence microscope (Carl Zeiss MicroImaging GmbH, Göttingen, Germany).

Photothermal Ablation of Cancer Cells with CuS NPs in Vivo. Nude mice were inoculated subcutaneously with 5×10^6 U87 cells in the right side of the rear leg 21 days before the experiment. When tumors had grown to 7−10 mm in diameter, mice were randomly allocated into five groups ($n = 5$). Mice in group A were injected intratumorally with PEG−CuS NPs (5 μL, 8 mM/mouse, 4×10^{13} NPs/mouse). Mice in groups B and C were injected intravenously with PEG−CuS NPs (200 μL, 8 mM/mouse). Mice in group D were injected intravenously with saline. Mice in group E did not receive any treatment. After 24 h, the tumors in mice from groups A, B, and D were irradiated with the NIR laser at 12 W/cm^2 for 5 min. The mice were killed 24 h after laser treatment, and tumors were removed, snap-frozen, and cryosectioned into 1000 μm slices. The slides were stained with hematoxylin/eosin. The slices were examined under a Zeiss Axio Observer.Z1 fluorescence microscope. The images were taken using a Zeiss AxioCam MRc5 color camera, and the extent of tumor necrosis (expressed as a percentage of the entire tumor area) was analyzed with Zeiss AxioVision software (version 4.6.3).

Statistical Analysis. Differences in biodistribution data and extent of necrosis (expressed as percentage of necrotic area after

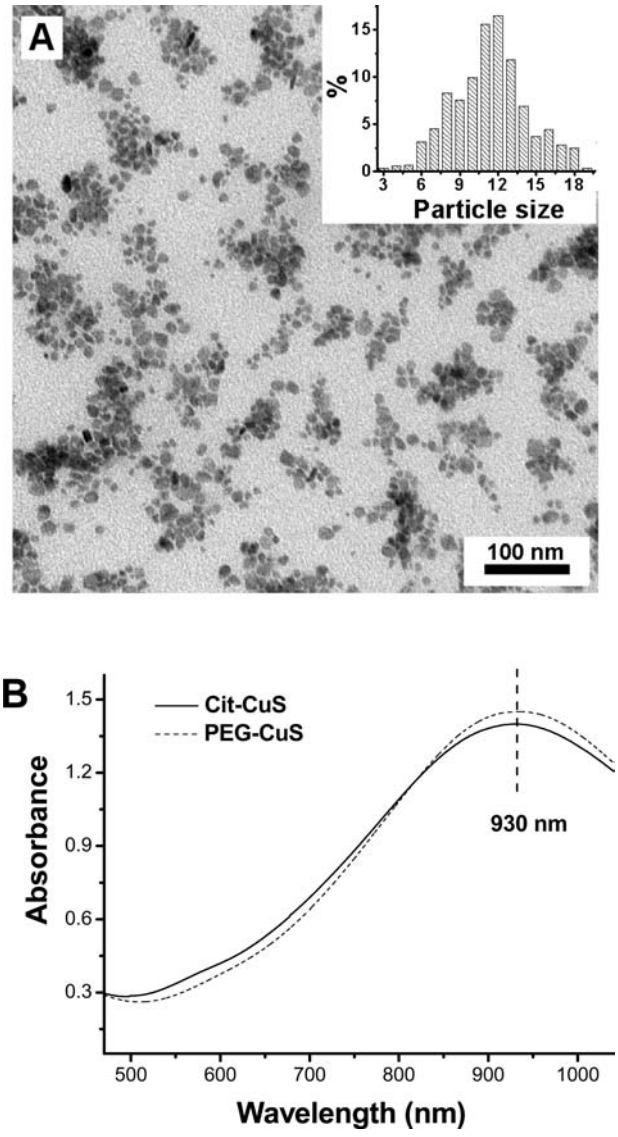

Figure 1. Characterization of CuS NPs. (A) TEM image of PEG−CuS NPs. Inset: particle size distribution. (B) Absorption spectra of Cit−CuS and PEG−CuS NPs.

treatments) were analyzed using the two-tailed Student's *t* test. Differences between groups were considered statistically significant at $p < 0.05$.

Results and Discussion

Synthesis, Characterization, and Stability. Citrate-coated CuS NPs (Cit−CuS NPs) were readily synthesized in aqueous solution by reacting $CuCl_2$ and Na_2S in the presence of sodium citrate at 90 °C for 15 min. The PEG coating was introduced by incubating Cit−CuS NPs with SH-PEG (molecular weight 5000 Da) at room temperature overnight. The coatings of citrate and PEG on the surface of the CuS NPs were confirmed using NMR analysis (Figure S1 in the Supporting Information). All of the X-ray diffraction peaks of the CuS NPs (Figure S2 in the Supporting Information) could be indexed as covellite-phase CuS with lattice parameters similar to those of Joint Committee on Powder Diffraction Standards card no. 79-2321. The diffraction peaks were relatively broad, reflecting the small size of the CuS crystals. No obvious impurity peaks were detected, indicating that covellite CuS was acquired with high quality. Figure 1A is a representative TEM image of the CuS NPs. The CuS NPs were well-dispersed and relatively uniform in size, with an average diameter of 11 nm. The hydrodynamic sizes of the CuS NPs were determined using dynamic light scattering (DLS) (Figure S3 in the Supporting Information). CuS NPs that had a TEM diameter of 11 nm showed a DLS size of 11.7 and 31.6 nm before and after PEG coating, respectively. The increased diameter of the PEG-coated NPs in aqueous solution was probably due to the PEG layer, which is invisible in TEM measurements. These CuS NPs were significantly larger than the previously reported thioglycolic acid-stabilized CuS NPs, which had an average diameter of 3 nm and displayed a peak absorbance at 900 nm.[35] HRTEM revealed the fringes of hexagonal CuS (102) planes with a lattice spacing of ∼0.3 nm (Figure S4 in the Supporting Information). These results are in agreement with the lattice spacing of the {102} planes (0.305 nm) of hexagonal CuS nanostructures described in previous reports.[36,37] The optical spectra of Cit−CuS and PEG−CuS NPs are shown in Figure 1B. Both types of NPs displayed a band-gap absorption that was blue-shifted relative to that of bulk CuS materials (peak at >1100 nm),[38] confirming the effect of quantum size confinement. On the basis of the measured absorbance *A*, the extinction coefficient was calculated to be $\sim 8.66 \times 10^7\ M^{-1}\ cm^{-1}$ at the peak absorption of 930 nm using the following equation:

$$\varepsilon = \frac{A\pi}{6d^3\rho N_A L C_{wt}}$$

where *d* is the average diameter of the CuS NPs assuming the NPs are spherical, ρ is the density of the NPs assuming it is the same as the bulk ($\sim 4.6\ g/cm^3$), N_A is Avogadro's constant, *L* is the path length (1 cm), and C_{wt} is the weight concentration of the NPs.

These are typical characteristics of covellite CuS and can be interpreted in terms of valence-band free carriers (positive holes), which are essentially metallic in character and give rise to NIR plasmon absorption because of their high charge density.[38] On the basis of the XRD, UV−vis spectroscopy, and TEM results, we concluded that we had made pure, high-quality CuS NPs. It is worth noting that the maximum absorption of the 11 nm Cit−CuS and PEG−CuS NPs (930 nm) is red-shifted by 30 nm relative to the absorption of the 3 nm CuS NPs previously reported by our groups[35] but blue-shifted by 50 nm relative to the absorption of the 15 nm CuS NPs previously reported by Zhao et al.,[38] who studied the composition dependence of plasmonic resonance spectra of $Cu_{2-x}S$. Future studies are needed to identify and clarify the effect of size on the NIR plasmonic resonance spectra of CuS NPs.

The stabilities of the Cit−CuS and PEG−CuS NPs were investigated by incubating these NPs in various media, including water, 0.4 mM citrate solution, 100 mM acetate buffer solution, 100 mM NaCl solution, HEPES buffer, PBS, 50 mM bovine serum albumin solution, PBS containing 10% FBS, and 100% FBS at 37 °C for up to 7 days. No precipitates were observed, and no obvious changes in hydrodynamic particle sizes were found for either type of NP in these solutions (Figure S5 and Table S1 in the Supporting Information), indicating that both

(36) Wu, C. Y.; Yu, S.-H.; Chen, S. F.; Liu, G. N.; Liu, B. H. *J. Mater. Chem.* **2006**, *16*, 3326–3331.
(37) Xu, H. L.; Wang, W. Z.; Zhu, W. *Mater. Lett.* **2006**, *60*, 2203–2206.
(38) Zhao, Y.; Pan, H.; Lou, Y.; Qiu, X.; Zhu, J.; Burda, C. *J. Am. Chem. Soc.* **2009**, *131*, 4253–4261.

Table 1. Radiolabeling Efficiency and Stability of [^{64}Cu]CuS NPs[a]

	Cit−[^{64}Cu]CuS NPs	PEG−[^{64}Cu]CuS NPs
CuS NPs	100%	100%
CuS NPs in PBS	87.3%	99.8%
CuS NPs in FBS	84.7%	99.2%

[a] Obtained using radio-ITLC after incubation in PBS or 100% FBS at 37 °C for 24 h.

the Cit−CuS and PEG−CuS NPs possess excellent colloidal stability under a wide range of environmental conditions.

[^{64}Cu]CuS NPs were prepared using the same procedures as for the preparation of plain CuS NPs, except that in the synthesis of PEG−[^{64}Cu]CuS NPs, the PEG coating was introduced directly during the course of CuS NP synthesis instead of after CuS NP formation through PEG/citrate substitution. This was necessary to shorten the time required for the synthesis of the [^{64}Cu]CuS NPs. The preparation of the 3 nm CuS NPs described in a previously reported procedure required more than 24 h for the reaction to reach completion at room temperature, which was not suitable for ^{64}Cu labeling because the decay half-life of ^{64}Cu is only 12.7 h. A high reaction temperature was used for rapid radiosynthesis of PEG−[^{64}Cu]CuS NPs, reducing the time required for PEG−[^{64}Cu]CuS NP production to ∼20 min. The specific activity was readily controlled by varying the radioactivity of $^{64}CuCl_2$ in the mixture of $^{64}CuCl_2$ and cold $CuCl_2$ at the time of [^{64}Cu]CuS synthesis. As shown in Table 1, 100% of the radioactivity was associated with Cit−[^{64}Cu]CuS NPs and PEG−[^{64}Cu]CuS NPs at the end of synthesis, indicating that the radiolabeling efficiency approached 100%. After incubation in PBS and FBS at 37 °C for 24 h, Cit−[^{64}Cu]CuS NPs lost 12.7 and 15.3% of their radioactivity, respectively. However, a negligible amount of radioactivity was lost from the PEG−[^{64}Cu]CuS NPs. These data indicated that ^{64}Cu was more stably integrated into PEG−[^{64}Cu]CuS NPs than Cit−[^{64}Cu]CuS NPs (Table 1 and Figure S6 in the Supporting Information).

Pharmacokinetics, Biodistribution, and PET Imaging. Blood activity−time profiles of Cit−[^{64}Cu]CuS and PEG−[^{64}Cu]CuS NPs are shown in Figure 2A, and the corresponding pharmacokinetic parameters are presented in Table 2. The two formulations appeared to have very different in vivo disposition characteristics. The mean systemic clearance was significantly slower with PEG (0.48 mL/h) than with citrate (0.75 mL/h, $p = 0.003$), suggesting that citrate-coated CuS NPs were cleared faster than PEG-coated CuS NPs following i.v. administration. This may be attributed to higher uptake by reticuloendothelial systems (RESs) (i.e., liver and spleen) and consequently faster elimination of Cit−[^{64}Cu]CuS NPs than of PEG−[^{64}Cu]CuS NPs. As a result, PEG−[^{64}Cu]CuS NPs had a significantly higher systemic exposure [i.e., area under the curve (AUC) = 213.7 %ID h/mL] than did Cit−[^{64}Cu]CuS NPs (134.9 %ID h/mL, $p = 0.008$). The mean volume of distribution at steady state, V_d(ss), was higher with citrate-coated NPs (5.8 mL) than with PEG-coated NPs (3.79 mL, $p = 0.018$), suggesting that citrate-coated NPs had higher uptake in such tissues as liver and spleen. Interestingly, there was no difference between the two CuS NP formulations with respect to the blood distribution half-life, $t_{1/2\alpha}$, and blood terminal elimination half-life, $t_{1/2\beta}$ (i.e., $t_{1/2\alpha}$ = 0.76 h and $t_{1/2\beta}$ = 5.98 h for Cit−[^{64}Cu]CuS NPs vs $t_{1/2\alpha}$ = 0.71 h and $t_{1/2\beta}$ = 6.06 h for PEG−[^{64}Cu]CuS NPs). This was likely due to the compensatory effect of systemic clearance and the volume of distribution. For each formulation, the volume of distribution at steady-state was close to the volume of distribution in the central compartment, V_c, indicating that the drug was mainly distributed to the central compartment (systemic blood circulation).

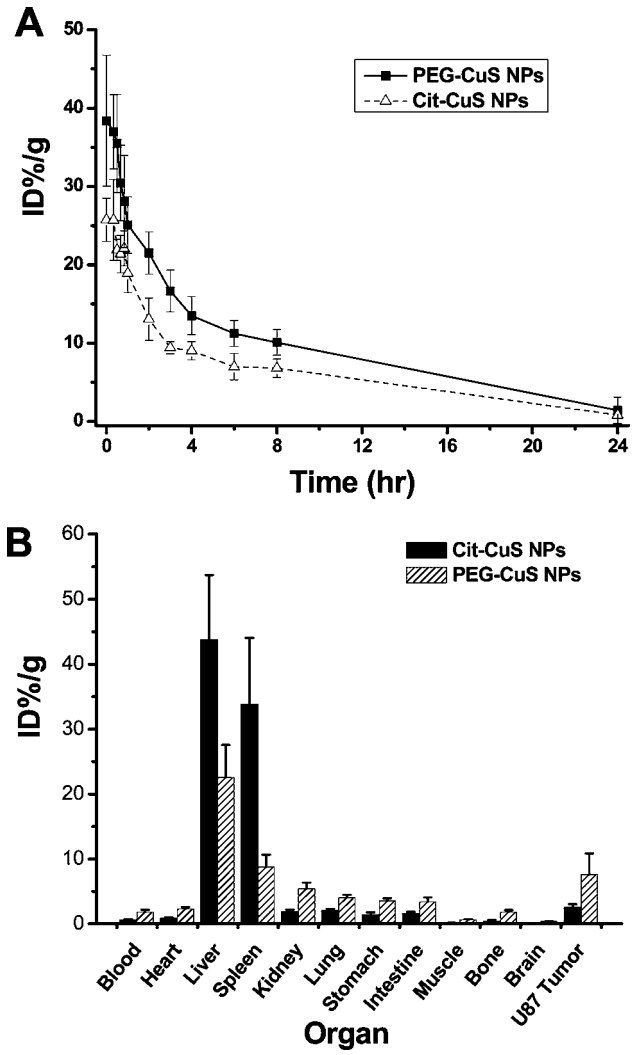

Figure 2. (A) Pharmacokinetic profiles of Cit−CuS NPs ($n = 3$) and PEG−CuS NPs ($n = 5$) following i.v. administration in mice and (B) biodistribution of Cit−CuS NPs ($n = 5$) and PEG−CuS NPs ($n = 5$) at 24 h after i.v. injection in mice bearing subcutaneous U87 glioma xenografts. Data represent means ± standard deviations.

Biodistribution data obtained 24 h after i.v. injection of Cit−[^{64}Cu]CuS NPs and PEG−[^{64}Cu]CuS NPs are shown in Figure 2B. Cit−[^{64}Cu]CuS NPs displayed significantly higher uptake than did PEG−[^{64}Cu]CuS NPs in the liver and the spleen, both of which are RES-enriched tissues. Conversely, PEG−[^{64}Cu]CuS NPs were less likely being captured by RES cells and therefore displayed higher levels in the heart, kidney, lung, stomach, intestine, and bone. These findings are consistent with the pharmacokinetic finding that PEG−[^{64}Cu]CuS NPs had slower systemic clearance than Cit−[^{64}Cu]CuS NPs, making them more available for distribution to target tissues. Importantly, uptake in human U87 glioblastoma xenografts in mice was almost 3 times as high with PEG−[^{64}Cu]CuS NPs as with Cit−[^{64}Cu]CuS NPs 24 h after i.v. injection (7.6 ± 1.4 %ID/g vs 2.6 ± 0.4 %ID/g, $p = 0.011$). This may be attributed to the enhanced permeability and retention effect of NPs and the greater systemic exposure of PEG−[^{64}Cu]CuS NPs, which made them more available for tumor uptake. This effect can be utilized for passive targeting of NPs to areas with increased angiogen-

Table 2. Pharmacokinetics Parameters of Cit−[^{64}Cu]CuS NPs and PEG−[^{64}Cu]CuS NPs after Intravenous Injection in Mice[a]

	$t_{1/2\alpha}$ (h)	$t_{1/2\beta}$ (h)	AUC (%ID h/mL)	V_d(ss) (mL)	V_c (mL)	CL (mL/h)	MRT (h)
Cit−[^{64}Cu]CuS NPs	0.76 ± 0.03	5.980.76 ± 0.030.35	134.90.76 ± 0.0315.56	5.800.76 ± 0.030.86	3.570.76 ± 0.030.22	0.750.76 ± 0.030.09	7.740.76 ± 0.030.32
PEG−[^{64}Cu]CuS NPs	0.710.76 ± 0.030.36	6.060.76 ± 0.031.58	213.70.76 ± 0.0332.36	3.790.76 ± 0.030.85	2.390.76 ± 0.030.56	0.480.76 ± 0.030.07	8.050.76 ± 0.031.90

[a] Values are means ± standard deviations. Abbreviations: $t^{\alpha}_{1/2}$, blood distribution half-life; $t^{\beta}_{1/2}$, blood terminal elimination half-life; AUC, area under the blood activity−time curve; V_d(ss), volume of distribution at steady-state; V_c, volume of distribution in the central compartment; CL, total body clearance; MRT, mean residence time.

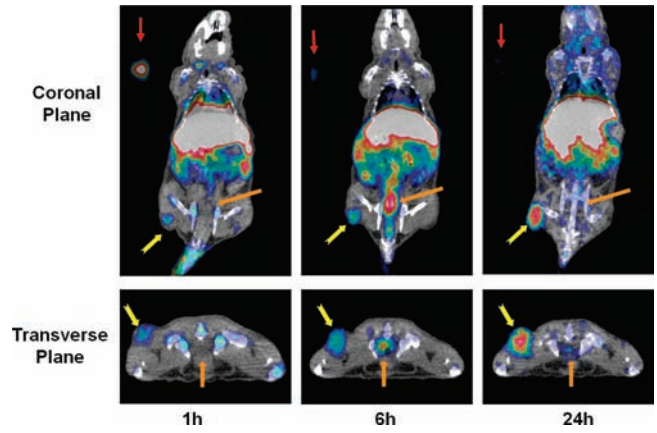

Figure 3. Micro-PET/CT images of nude mice bearing subcutaneous U87 glioma xenografts acquired at 1, 6, and 24 h after i.v. injection of PEG−[^{64}Cu]CuS NPs. Yellow arrow, tumor; orange arrow, bladder; red arrow, standard.

esis, where NPs with longer blood circulation times exhibit higher tumor uptake.[9,15]

Because they had greater radiolabel stability and a higher tumor uptake value than the Cit−[^{64}Cu]CuS NPs, the PEG−[^{64}Cu]CuS NPs were further evaluated with regard to their utility for in vivo PET. Figure 3 shows representative whole-body micro-PET/CT images of a mouse acquired at 1, 6, and 24 h after i.v. injection of PEG−[^{64}Cu]CuS NPs. Consistent with the biodistribution analysis, PET/CT images revealed high uptake of PEG−[^{64}Cu]CuS NPs in the liver and spleen. As expected, PEG−[^{64}Cu]CuS NPs gradually accumulated in the tumor between 1 and 24 h, permitting remarkably clear visualization of the tumor 24 h after injection. Quantitative analysis showed that the average tumor-to-muscle ratios at 1, 6, and 24 h after NP injection were 2.74:1, 6.14:1, and 6.55:1, respectively, indicating that PEG−[^{64}Cu]CuS NPs were deposited and retained in the tumor over the 24 h period. These values compared favorably with those for ^{64}Cu-labeled quantum dots targeted to integrin $\alpha_v\beta_3$ receptors, where RGD-coated quantum dots were found to have a tumor-to-muscle ratio of 4:1 at 5 h after i.v. injection into nude mice with U87 tumors.[7] PEG−[^{64}Cu]CuS NPs were excreted by both renal and hepatobiliary routes, as indicated by the deposition of radioactivity in the bladder and the gastrointestinal tract (Figure 3). ITLC analysis revealed that PEG−[^{64}Cu]CuS NPs were cleared from the renal system in the form of NPs (Figure S7 in the Supporting Information). A previous study by Choi et al.[39] with quantum dots demonstrated that NPs smaller than 5 nm can be cleared by the renal route. Although the average diameter of the CuS NPs was 11 nm, it is possible that a small fraction of the CuS NPs smaller than 5 nm in diameter were capable of renal clearance.

In Vitro and in Vivo Photothermal Therapy. To date, there have been few reports on NPs smaller than 20 nm having NIR absorption.[35] The smallest gold nanostructures reported to date to have plasmon NIR absorptions were ~40 nm in diameter.[8,29] Because the pharmacokinetics and biodistribution pattern of NPs are strongly affected by their size,[9,15] it is highly desirable that novel nanostructures having diameters of less than 20 nm with NIR absorption be identified and evaluated. CuS NPs, which are much smaller than gold nanostructures, may have a better

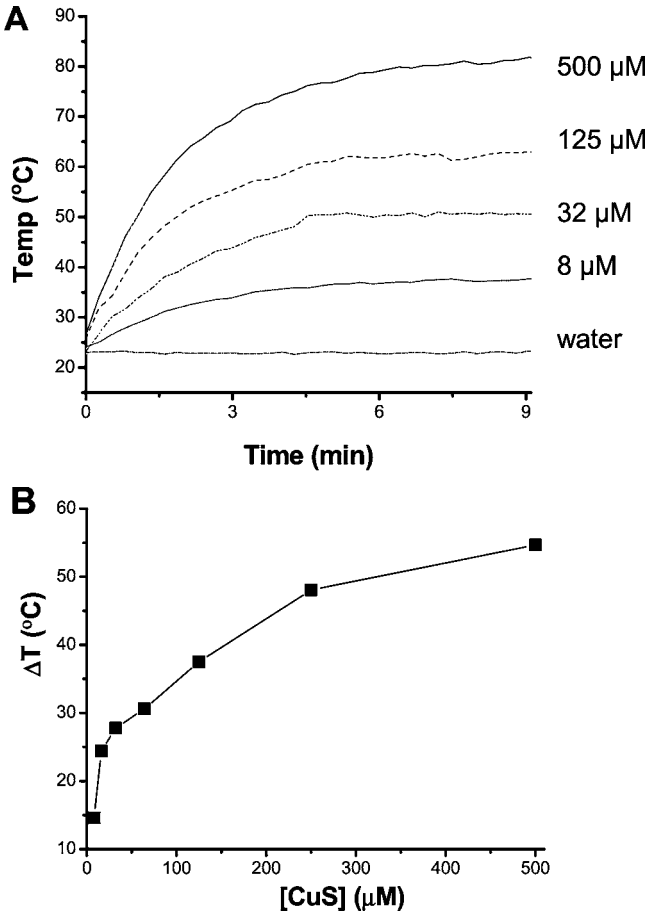

Figure 4. PEG−CuS NPs can act as an efficient photothermal coupling agent. (A) Temperature elevation over a period of 9 min of exposure to NIR light (16 W/cm^2) at various PEG−CuS NP concentrations. Water was used as a control. (B) Temperature change (ΔT) over a period of 9 min as a function of PEG−CuS NP concentration expressed as CuS molecular units.

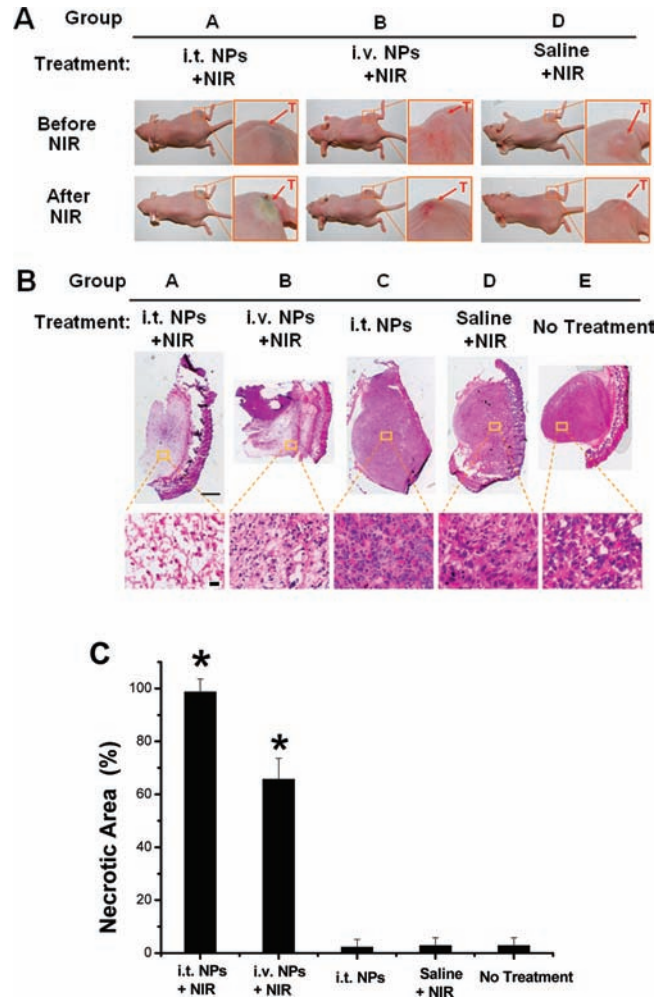

Figure 5. PEG−CuS NPs can induce photothermal destruction of U87 tumors in vivo. (A) Photographs of tumor-bearing mice before and at 24 h after NIR laser irradiation (12 W/cm^2 at 808 nm for 5 min). (B) Representative microphotographs of tumors removed 24 h after NIR laser treatment. The tissues were cryosectioned into 5 μm slices and stained with hematoxylin/eosin. Upper scale bar, 200 μm; lower scale bar, 20 μm. (C) Quantitative analysis of the percentage of necrosis zone induced by various treatments. The data were measured as a percentage of the whole tumor area. Asterisks indicate statistical significance relative to the no-treatment control ($p = 0.006$). Error bars represent standard deviations ($n = 5$). Abbreviations: i.t, intratumoral injection; i.v., intravenous injection; NPs, CuS nanoparticles; NIR, near-infrared laser; T, tumor.

chance of reaching their targets and being cleared from the body through the renal system.[9,39,40]

An important feature of CuS NPs is their NIR light-induced thermal effect, which could be used for PTA therapy. To investigate the temperature elevation induced by NIR laser irradiation in the presence of CuS NPs, we used a continuous-wave fiber-coupled diode laser centered at 808 nm. Figure 4A shows the temperature change of an aqueous solution containing PEG−CuS NPs as a function of exposure time. Exposure of an aqueous solution of PEG−CuS NPs [500 μM CuS molecular units, 7.1×10^{14} particles/mL (23 nM CuS NPs)] to the NIR laser light (16 W/cm^2) for 5 min elevated the temperature of the solution from 25 to 80 °C (an increase of 55 °C). Under the same conditions, no change in temperature was observed with pure water. The magnitude of the increase in the temperature of the aqueous solution of PEG−CuS NPs decreased with decreasing PEG−CuS NP concentration (Figure 4B). These data indicate that PEG−CuS NPs can act as an efficient photothermal coupling agent. In comparison with our previously reported 3 nm CuS NPs,[35] the new 11 nm CuS NPs displayed a higher photothermal conversion efficiency. For example, the temperature of an aqueous solution of 3 nm CuS NPs increased by 12.7 °C over a period of 5 min at an output power of 24 W/cm^2 and a concentration of 770 μM CuS units ($\sim 4.8 \times 10^{16}$ particles/mL).[35]

To test the cell killing induced by the photothermal effect through CuS NPs, human U87 glioblastoma cells were incubated with PEG−CuS NPs for 2 h. The cells were then irradiated with the NIR laser centered at 808 nm. The cell viability after exposure to the NIR laser was probed using calcein AM dye, which reports ubiquitous intracellular esterase activity. At 24 h after laser treatment, cells treated with PEG−CuS NPs at a concentration of 500 μM CuS plus the NIR laser (16 W/cm^2 for 5 min, 40 W/cm^2 for 2 min, or 40 W/cm^2 for 5 min) had substantially reduced cell densities (Figure S8 in the Supporting Information). No apparent change in cell viability was observed when cells were treated with CuS NPs alone at 100 μM or 500

(39) Choi, H. S.; Liu, W.; Misra, P.; Tanaka, E.; Zimmer, J. P.; Itty Ipe, B.; Bawendi, M. G.; Frangioni, J. V. *Nat. Biotechnol.* **2007**, *25*, 1165–1170.
(40) Burns, A. A.; Vider, J.; Ow, H.; Herz, E.; Penate-Medina, O.; Baumgart, M.; Larson, S. M.; Wiesner, U.; Bradbury, M. *Nano Lett.* **2009**, *9*, 442–448.

μM or the NIR laser alone at 16 W/cm^2 for 5 min or 40 W/cm^2 for 5 min. These results indicated that PEG−CuS NPs mediated the photothermal destruction of U87 cells.

In mice bearing subcutaneous U87 tumors, the skin of the mice at the tumor site turned greenish after both i.t. and i.v. injection of PEG−CuS NPs as a result of the deposition of the NPs in the tumor (Figure 5A). After NIR irradiation, the skin at the tumor sites in mice that received i.t. injection as well as in mice that received i.v. injection of PEG−CuS NPs turned brownish or dark-red, indicating tissue burns caused by the local photothermal effect. In contrast, there was no noticeable change in the skin of mice treated with PEG−CuS NPs alone, saline plus NIR irradiation, or the NIR laser alone (Figure 5A).

Histological examination confirmed that the combination of PEG−CuS NPs administered by either i.t. or i.v. injection followed by laser treatment caused significantly greater necrotic response than did PEG−CuS NPs without laser treatment, saline plus laser treatment, or saline only (Figure 5B). In the mice treated with PEG−CuS NPs plus the laser, common features of thermonecrosis such as loss of nucleus, cell shrinkage, and coagulation were found in the tumor tissues. In the mice treated with i.t. injection of PEG−CuS NPs plus the laser, almost all of the tumor tissue was necrotized, exhibiting pyknosis, karyolysis, cytoplasmic acidophilia, and degradation and corruption of the extracellular matrix of the tumor. In the mice treated with i.v. injection of PEG−CuS NPs plus the laser, ∼65% of the tumor tissue was necrotized. In the mice treated with saline plus laser, there was only a baseline fraction of necrosis in tumor tissue (<5%). In the tumors of mice treated with CuS NPs alone (i.t. injection), saline plus NIR laser, or saline alone, there was little pyknosis or karyolysis, confirming the benign nature of these treatments (Figure 5C). Thus, selective in vivo photothermal destruction of the tumors mediated by PEG−CuS NPs was confirmed.

Conclusions

In summary, PEG−[^{64}Cu]CuS NPs can act as an efficient radiotracer for pharmacokinetics, biodistribution, and PET imaging, and PEG−CuS NPs can act as an efficient photothermal coupling agent. The combination of small size, strong absorption in the NIR region, and integration of the positron emitter ^{64}Cu into the core structural component makes [^{64}Cu]CuS NPs ideally suited for theranostic applications (i.e., image-guided PTA therapy). PEG−[^{64}Cu]CuS NPs showed high uptake in U87 human glioblastoma xenografts as a result of enhanced permeability and retention effects. Future studies will focus on active targeting of [^{64}Cu]CuS NPs to solid tumors by conjugating receptor-specific targeting moieties onto the NPs' surface. Improved tumor uptake of PEG−[^{64}Cu]CuS NPs should increase the efficacy of photothermal ablation therapy, decrease the energy dose of the laser, and minimize the potential damage to surrounding normal tissues. In addition to serving as a photothermal mediator, [^{64}Cu] and potentially [^{67}Cu]-labeled CuS NPs may also have an application in radiotherapy. Thus, the multifunctional [^{64}Cu]CuS NPs combining intrinsic nuclear and optical properties for PET imaging and photothermal therapy represent a new nanoplatform for theranostic applications.

Acknowledgment. We thank Stephanie Deming for editing the article and Qian Huang and Meng Zhong for helping with animal and cell-culture studies. We also thank Professor Wei Chen (The University of Texas at Arlington) for helpful discussions. This work was supported in part by National Institutes of Health Cancer Center Support Grant CA016672, National Institutes of Health Grant R01 CA119387, a seed grant through the Alliance for NanoHealth by the U.S. Department of Army Telemedicine and Advanced Technology Research Center (W81XWH-07-2-0101), the John S. Dunn Research Foundation, and Shanghai Leading Academic Discipline Projects, China (S30203) (to S.S.).

Supporting Information Available: Complete refs 17 and 31; NMR, XRD, HRTEM, and DLS characterization data for CuS NPs; stability and radiolabeling efficiency of CuS NPs; and results of in vitro PTA therapy studies. This material is available free of charge via the Internet at http://pubs.acs.org.

JA106855M